Study of the influence between magnesium ions and calcium ions on the morphology and size of coprecipitation in microemulsion

Nong Wang[1,2], *Lijuan Yang*[1], *Lixuan Chen*[1], *Rong Xiao*[1]

[1]*School of Chemical and Biological Engineering, Lanzhou Jiaotong University, Lanzhou 730070, People's Republic of China*
[2]*Engineering and Technology Center of Gansu Province for Botanical Pesticides, Lanzhou Jiaotong University, Lanzhou 730070, People's Republic of China*
E-mail: wangnong07@163.com

Published in Micro & Nano Letters; Received on 6th November 2013; Revised on 2nd March 2014; Accepted on 21st March 2014

A series of inverse-microemulsion quasi-ternary system phase diagrams of CTAB + *n*-butanol + *n*-hexane + brine ($MgCl_2/CaCl_2$) is systematically drawn by adjusting the ratio of $MgCl_2$ and $CaCl_2$. On this basis, a microemulsion has been prepared with five different molar ratios of magnesium ions to calcium ions, and a calcium carbonate and magnesium carbonate coprecipitation product is obtained by reaction with an equimolar amount of sodium carbonate. The samples were characterised by scanning electron microscopy (SEM), a Fourier transform infrared (FTIR) spectrometer and X-ray diffraction (XRD). The SEM photographs indicated that when the content of Ca^{2+} was higher, some large fusiform aggregates of coprecipitation particles were formed in solution, but with the content of Mg^{2+} increased gradually, they eventually formed small and uniform sphere particles. The measurement results of XRD and FTIR indicated that the crystal structures of calcium carbonate in coprecipitation changed gradually from vaterite into aragonite and finally turned into being amorphous with the increasing of the proportion of magnesium ions.

1. Introduction: Calcium carbonate is the main substance in limestone which has numerous uses: as a building material, as aggregate for the base of roads, as white pigment or filler in products such as toothpaste or paints, and as a chemical feedstock. Calcium carbonate also abounds in biological fields [1, 2], and is the main component of coral, mollusks, exoskeletons and many crustaceans. Usually, there are various forms of calcium carbonate, three common anhydrous crystallines are calcite, aragonite and vaterite. In addition, six hydrated calcium carbonate, hydrated calcium carbonate and amorphous forms rarely exist in nature because of their thermodynamic instability which is often used as intermediate reactions. The amorphousness is very special, and can be divided into two types: stable amorphous calcium carbonate and the unstable amorphous calcium carbonate [3]. They play a very important role in the organism and crystallisation behaviour. As a non-crystal the former is stable in the organism, whereas the latter is the precursor of forming calcite and aragonite.

Magnesium carbonate is a kind of important magnesium inorganic chemical product. It is mainly used as an industrial intermediate material, calcining the precursor for the preparation of high-purity magnesite clinker or magnesium oxide. Magnesium carbonate whisker as a kind of typical functional product of magnesium carbonate, is a single crystal of hydrated magnesium carbonate, containing less defects, having less impurity and its strength is close to the ideal crystals. It can be used as the composite filler, such as used in plastics, rubber, paint and printing ink, and exhibits excellent physical and chemical properties and excellent mechanical properties.

The microemulsion method is an effective process for the preparation of nanoparticles which has been developed in recent years. As early as 1959, the term microemulsion was proposed by Schulman *et al.* [4]. The microemulsion method is widely used as a template for the preparation of nanomaterials because of its simple operation, it does not need to be calcined at high-temperature, it does not need special equipment and the size can be adjusted by changing its composition and so on. Microemulsion medium used as the preparation method of nanomaterials has been widely used in the preparation of composite catalyst and other semiconductors [5, 6], superconductors [7], magnetic nanoparticles [8, 9] and so on. Owing to the different compositions having different stable ranges of the microemulsion system, it is necessary to study the stability region of the microemulsion system for the preparation of nanoparticles.

In nature and biology, we can see the coexistence of magnesium carbonate and calcium carbonate, with many containing magnesium from levels of a few per cent up to 44% [10–12]. Some studies indicated that Mg^{2+} played an important part in the biomimetic mineralisation process of $CaCO_3$ [13, 14]. Studies have also shown that Mg^{2+} ions can significantly change the morphology of calcium carbonate crystals, which played an extremely important role in the formation of calcium carbonate aragonite [15–22]. For example, they can affect the metabolism of bone tissue by affecting the secretion of thyroid hormone synthesis, and the regulation of calcium in the bones inside and outside activities. Magnesium deficiency is the most common manifestation of premature aging of bones, osteoporosis and soft tissue calcification. Because the formation and growth of bone is completed in organisms which is a relatively closed system, and has some similarities to the formation of calcium carbonate in the oil-in-water microemulsion, we therefore study the effect of Mg^{2+} in microemulsion on calcium carbonate morphology to explore the effect mechanism of Mg^{2+} on the formation of calcium carbonate in a closed system.

In the work reported in this Letter, we studied systematically the microemulsion region of the quasi-ternary system phase diagram of hexadecyl trimethyl ammonium bromide (CTAB)/*n*-butanol/*n*-hexane/brine ($MgCl_2/CaCl_2$) system and obtained different morphologies and crystal structures of the product by adjusting the proportion of calcium ions to magnesium ions. On this basis, we found Mg^{2+} has an important influence on the shape and appearance of calcium carbonate in microemulsion. These results can help us to understand the effect mechanism of Mg^{2+} on the formation of calcium carbonate and the synthesising of special and new functional materials.

2. Experimental material and methods

2.1. Reagent and instrument: Hexadecyl trimethyl ammonium bromide ($C_{16}H_{33}N(CH_3)_3Br$, referred to as CTAB), is a kind of cationic surfactant, as received (AR); *n*-butyl alcohol (*n*-C_4H_9OH) is used as a surface active agent, AR; hexane (*n*-C_6H_{14}) is used as the oil phase, AR; anhydrous calcium chloride, magnesium

doi: 10.1049/mnl.2013.0656

Table 1 Composition of phase formation point and phase vanishing point

$MgCl_2$	Phase formation point			Phase vanishing point		
	m_s	m_o	m_a	m_s	m_o	m_a
	10	0	1.4555	10	0	5.6514
	9	1	1.1686	9	1	4.0576
	8	2	0.9582	8	2	3.1689
	7	3	0.8024	7	3	2.5543
	6	4	0.6011	6	4	2.0202
	5	5	0.5092	5	5	1.4649
	4	6	0.4757	4	6	1.0792
	3	7	0.3425	3	7	0.8946
	2	8	0.2863	2	8	0.7194
	1	9	0.2358	1	9	0.5686
	0	10	0	0	10	—
$CaCl_2$						
	10	0	1.1175	10	0	5.0833
	9	1	0.9841	9	1	3.638
	8	2	0.8916	8	2	2.932
	7	3	0.567	7	3	2.1777
	6	4	0.5533	6	4	1.9295
	5	5	0.4172	5	5	1.5107
	4	6	0.386	4	6	1.2109
	3	7	0.3262	3	7	1.0207
	2	8	0.2694	2	8	0.7445
	1	9	0.1733	1	9	0.7536
	0	10	0	0	10	—

By which the quasi-ternary system phase diagrams of microemulsion region with 1 mol/l magnesium chloride and 1 mol/l calcium chloride aqueous solution was drawn, respectively

chloride hexahydrate, AR; sodium carbonate AR; and double-distilled water, were also used.

The morphology was analysed by scanning electron microscopy (SEM) (JSM-6701F, JEOL Ltd, Japan).

The samples (in proportions of 1% in KBr powder) were prepared and recorded with a Fourier transform infrared (FTIR) spectrometer Shimabzu-IR Prestige-21 between 4000 and 400 $cm^{-1}$with a resolution of 2 cm^{-1}.

The X-ray diffraction (XRD) data were measured by using XRD-7000LX (Shimadzu, Japan). The XRD data were recorded over the 2θ range of 0°–60° with a step size of 0.002°. Identification of phases was carried out by comparing the diffraction patterns with the standard PDF cards.

2.2. Microemulsion quasi-ternary system phase diagram drawing: CTAB and *n*-butanol mixed at the mass ratio of 1:2 were treated as one component, and a series of quasi-two-component systems by mixing with the *n*-hexane at different accurate mass ratios (0:10, 1:9, 2:8, 3:7, 4:6, 5:5, 6:4, 7:3, 8:2, 9:1 and 10:0) were added into a 50 ml conical flask with a cover. The total mass of each mixed sample is approximately 10 g and all samples were stored in a thermostatic water bath at 25 ± 1°C for 2 h.

The 1.0 M aqueous solution of $MgCl_2$ and a 1.0 M aqueous solution of $CaCl_2$ were prepared, then the $MgCl_2/CaCl_2$ mixed aqueous solution at different molar ratios of 1:3, 1:2, 1:1, 2:1 and 3:1 with the total concentration of 1 M were prepared. $MgCl_2/CaCl_2$ aqueous solutions with different proportions were added slowly by dropping them into the CTAB/*n*-butanol + *n*-hexane quasi-two-component system phase transition points have been determined through visual observation. When the system changes from turbid to clear, the microemulsion phase formation point can be determined, we then continued to add more $MgCl_2/CaCl_2$ aqueous solution, until the system changed from clear to turbid; the microemulsion vanishing point can then be determined. After each change of the system, we waited at least 2 h for the system to establish a new equilibrium before the new data were taken. We found that when the system was close to the phase point, the time for the equilibrium was longer than 1 h. The compositions of the phase transformation point were determined by measuring the amount of water added for each system at 25 ± 1°C. The microemulsion phase formation point and the microemulsion phase vanishing point with 1 mol/l magnesium chloride and 1 mol/l calcium chloride aqueous solution are listed in Table 1, by which the quasi-ternary system phase diagrams of CTAB/*n*-butanol + *n*-hexane + brine ($CaCl_2$ and $MgCl_2$) drawn by Origin software are shown in Fig. 1. From Figs. 1*a* and *b*, we can see that the microemulsion region phase diagram of $CaCl_2$ and $MgCl_2$ are very similar, and both $CaCl_2$ and $MgCl_2$ have a large area of microemulsion, since both $MgCl_2$ and $CaCl_2$ have a strong ability to combine with water.

At the same time, we also draw quasi-ternary system phase diagrams of CTAB/*n*-butanol + *n*-hexane + brine ($CaCl_2 + MgCl_2$) with different proportions of $MgCl_2/CaCl_2$; the data are listed in Table 2 and as shown in Fig. 2. Different proportions of the $MgCl_2/CaCl_2$, CTAB, *n*-butanol and *n*-hexane microemulsion systems also have similar microemulsion phase diagrams. We calculated the microemulsion region area of the $MgCl_2/CaCl_2$ mixed aqueous solution at different mass ratios by using Image-Pro Plus software, and we found the areas fluctuated within a range of 14 000–17 000 with similar graphical shapes, see Fig. 3. These microemulsion region phase diagrams provide a

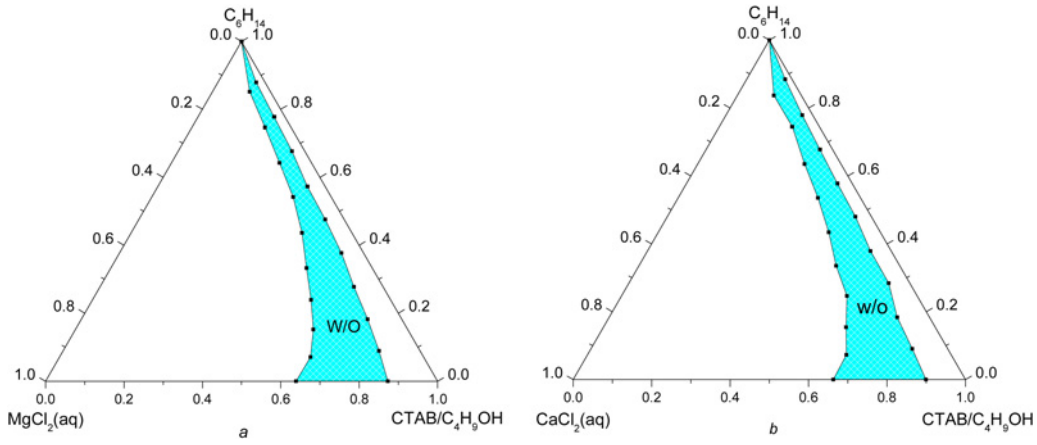

Figure 1 *Quasi-ternary system inverse-microemulsion region phase diagram of CTAB + n-butanol + n-hexane + brine ($MgCl_2/CaCl_2$)*
a 1 mol/l magnesium chloride aqueous solution
b 1 mol/l calcium chloride aqueous solution

Table 2 Composition of phase formation point and phase vanishing point

Mg^{2+}:Ca^{2+}	Phase formation point			Phase vanishing point		
	m_s	m_o	m_a	m_s	m_o	m_a
1:3	10	0	1.3699	10	0	4.5874
	9	1	0.9510	9	1	3.6273
	8	2	0.6664	8	2	2.6573
	7	3	0.5553	7	3	2.1552
	6	4	0.3272	6	4	1.8037
	5	5	0.3091	5	5	1.4219
	4	6	0.2524	4	6	1.0693
	3	7	0.2163	3	7	0.9635
	2	8	0.1663	2	8	0.7260
	1	9	0.1026	1	9	0.5764
	0	10	0	0	10	—
1:2	10	0	1.1154	10	0	4.2022
	9	1	0.9148	9	1	3.4034
	8	2	0.5776	8	2	2.4726
	7	3	0.5199	7	3	2.1293
	6	4	0.3198	6	4	1.7504
	5	5	0.2764	5	5	1.3855
	4	6	0.2480	4	6	1.0239
	3	7	0.1975	3	7	0.8678
	2	8	0.1561	2	8	0.6834
	1	9	0.0827	1	9	0.5689
	0	10	0	0	10	—
1:1	10	0	0.9714	10	0	4.0760
	9	1	0.7089	9	1	2.8549
	8	2	0.4654	8	2	2.3968
	7	3	0.3681	7	3	1.9321
	6	4	0.3158	6	4	1.4346
	5	5	0.2705	5	5	1.1814
	4	6	0.2054	4	6	0.9156
	3	7	0.1741	3	7	0.7397
	2	8	0.1396	2	8	0.6171
	1	9	0.0787	1	9	0.3369
	0	10	0	0	10	—
2:1	10	0	1.3696	10	0	5.5550
	9	1	0.9326	9	1	3.9341
	8	2	0.8082	8	2	3.0416
	7	3	0.5765	7	3	2.1256
	6	4	0.4246	6	4	1.8118
	5	5	0.3856	5	5	1.3575
	4	6	0.2992	4	6	1.0577
	3	7	0.2562	3	7	0.9111
	2	8	0.1789	2	8	0.7214
	1	9	0.1029	1	9	0.5485
	0	10	0	0	10	—
3:1	10	0	1.2768	10	0	5.6178
	9	1	1.0430	9	1	3.9723
	8	2	0.7411	8	2	3.0039
	7	3	0.5955	7	3	2.4205
	6	4	0.4285	6	4	1.9124
	5	5	0.4853	5	5	1.4032
	4	6	0.3149	4	6	0.9599
	3	7	0.2913	3	7	0.8883
	2	8	0.2250	2	8	0.6730
	1	9	0.1329	1	9	0.5165
	0	10	0	0	10	—

By which the quasi-ternary system phase diagrams of microemulsion region with different Mg^{2+}/Ca^{2+} ratio were drawn.
m_s represents surfactant CTAB and cosurfactant *n*-butanol, in which their mass ratio is 1:2; m_o represents the mass of *n*-hexane; and m_a represents the mass of magnesium chloride and calcium chloride mixed aqueous solution

theoretical guidance for the preparation of the reverse microemulsions and the preparation of nanoparticles with controllable size and morphology.

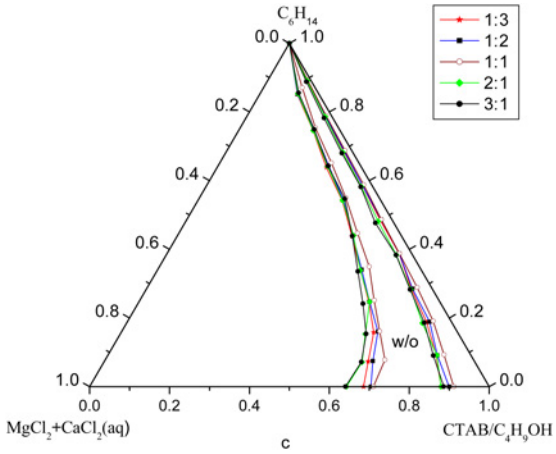

Figure 2 *Quasi-ternary system inverse-microemulsion region phase diagram of CTAB + n-butanol + n-hexane + brine ($MgCl_2$/$CaCl_2$) with different mass ratios of $MgCl_2$ and $CaCl_2$*
Different symbols represent different mass ratios of magnesium chloride to calcium chloride, filled star – 1:3, filled square – 1:2, open circle – 1:1, filled diamond – 2:1 and filled circle – 3:1

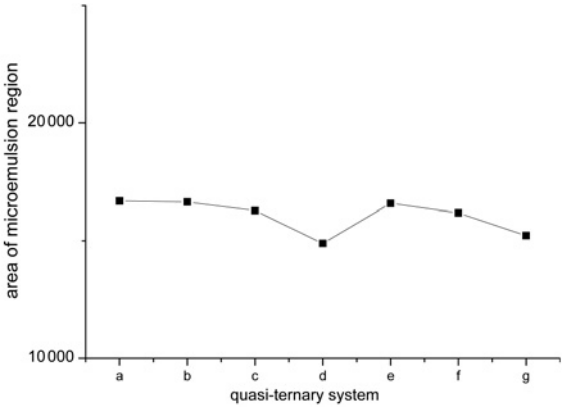

Figure 3 *Relative area of inverse-microemulsion region of the quasi-ternary system inverse-microemulsion region phase diagram of CTAB + n-butanol + n-hexane + brine ($MgCl_2$/$CaCl_2$) with different mass ratio of $MgCl_2$ and $CaCl_2$*
a Ca^{2+}, b 1:3, c 1:2, d 1:1, e 2:1, f 3:1, g Mg^{2+}

2.3. Nanometre calcium carbonate preparation: In the experimental process, a mixed solution was prepared by the dissolving of CTAB and *n*-butylalcohol at the mass ratio of 1:2, then mixed with *n*-hexane at the mass ratio of 5:5 in a 50 ml conical flask. After about 30 min of dissolving, a 1.0 M $MgCl_2$/$CaCl_2$ mixture aqueous solution with different molar proportions of 3:1, 2:1, 1:1, 1:2 and 1:3 was added.

$CaCO_3$ and $MgCO_3$ were crystallised via a reaction between an equimolar Na_2CO_3 aqueous solution and a $CaCl_2$/$MgCl_2$ microemulsion solution. The reactant solutions were mixed in a reactor with a stirring rate that was fixed at 700 rpm. All the experimental studies were performed at a 25 ± 1° temperature. Normally, the crystallisation was finished after the reactants were mixed for 1 h. The suspension was aged for about 12 h, and purified by centrifugation (at a rate of 15 000 rpm). The suspension was centrifuged twice to ensure that the particles were well purified. Ethanol was used to wash the centrifuged particles twice. Finally, the samples were completely dried at a temperature of 60°C under atmospheric conditions.

3. Results and discussion: The FTIR spectra of calcium carbonate were mainly FTIR absorption peaks of CO_3^{2-} which were divided

doi: 10.1049/mnl.2013.0656

into four regions at around v_1 ~1080 cm^{-1}, v_3 ~1450 cm^{-1}; v_2 ~870 cm^{-1} and v_4 ~700 cm^{-1}; an among these v_2 was an in-plane bending vibration absorption peak and v_4 was an out-plane bending vibration absorption peak. Different forms of calcium carbonate have different characteristic absorption peaks as follows: calcite, ~875 and ~713 cm^{-1}; aragonite, ~856, ~713 and ~700 cm^{-1} (weak); vaterite, 875 and 745 cm^{-1}. Owing to the disorderly absorption peak structure, amorphous calcium carbonate appears at ~860 cm^{-1} with the absorption peak width increasing obviously [23, 24]. Hence, FTIR spectroscopy is an effective tool for characterising amorphous calcium carbonate and monitoring its transformation, and the difference of calcium carbonate can be distinguished by using the infrared absorption peak position that appeared.

Figs. 4*a* and *b* show that the characteristic absorption peaks occurred at 875, 856, 745, 712 and 700 cm^{-1} (weak) which indicate that the product is a mixture of calcite and aragonite and vaterite. Fig. 4*c* shows that the characteristic absorption peaks occurred at 875, 856, 713 and 700 cm^{-1} (weak) which indicate that the product is a mixture of calcite and aragonite. Figs. 4*d* and *e* show that there are broad and strong absorption peaks at 860 cm^{-1}, no absorption at 713 or 745 cm^{-1} which also show that the calcium carbonate particle are amorphous calcium carbonate [25, 26]. We found that with the proportion of magnesium ions enhanced, the content of aragonite increased gradually, whereas the content of calcite decreased in the product.

Fig. 5 shows SEM and XRD images of coprecipitation particles depending on reverse micelle systems with different Mg^{2+}/Ca^{2+} proportions. Through observation of the five groups of the SEM data, we can see that the coprecipitation particles were prepared. It can be found that with the change of the proportion of magnesium ions to calcium ions, the morphology and size of calcium carbonate will be changed, and the size of the particles decrease with the increase of the proportion of magnesium ions to calcium ions. When Mg^{2+} to Ca^{2+} have a ratio of 1:3, the spindle and shell calcium carbonate particles mainly formed, with the proportion of magnesium ions to calcium ions enhanced to 2:1, the spindle and shell particles decrease and the spherical particles increase. Finally, with the proportion of magnesium ions to calcium ions enhanced to 3:1, the spindle and shell particles disappeared and all of the spherical particle are obtained. After an abortive observation, we found that the spindle and shell particles are also aggregates of small particles which were about 10–100 nm. The coprecipitation of calcium carbonate and $Mg_5(CO_3)_4(OH)_2 \bullet 4H_2O$ were prepared by the microemulsion of a mixture of $CaCl_2$ and $MgCl_2$. Our previous research has shown that selecting suitable ω_0 values can result in the formation

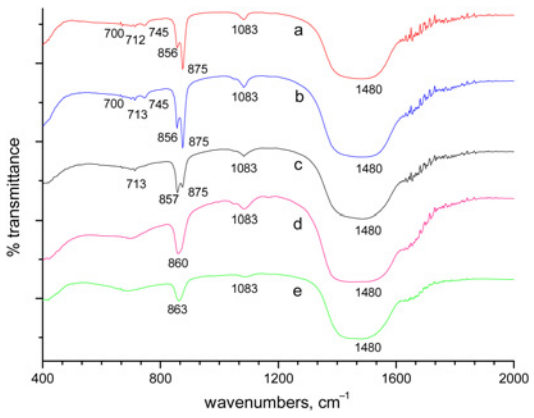

Figure 4 *Infrared spectra of coprecipitation particles depending on reverse micelle systems with different Mg^{2+}/Ca^{2+} ratios*
a 1:3, b 1:2, c 1:1, d 2:1, e 3:1

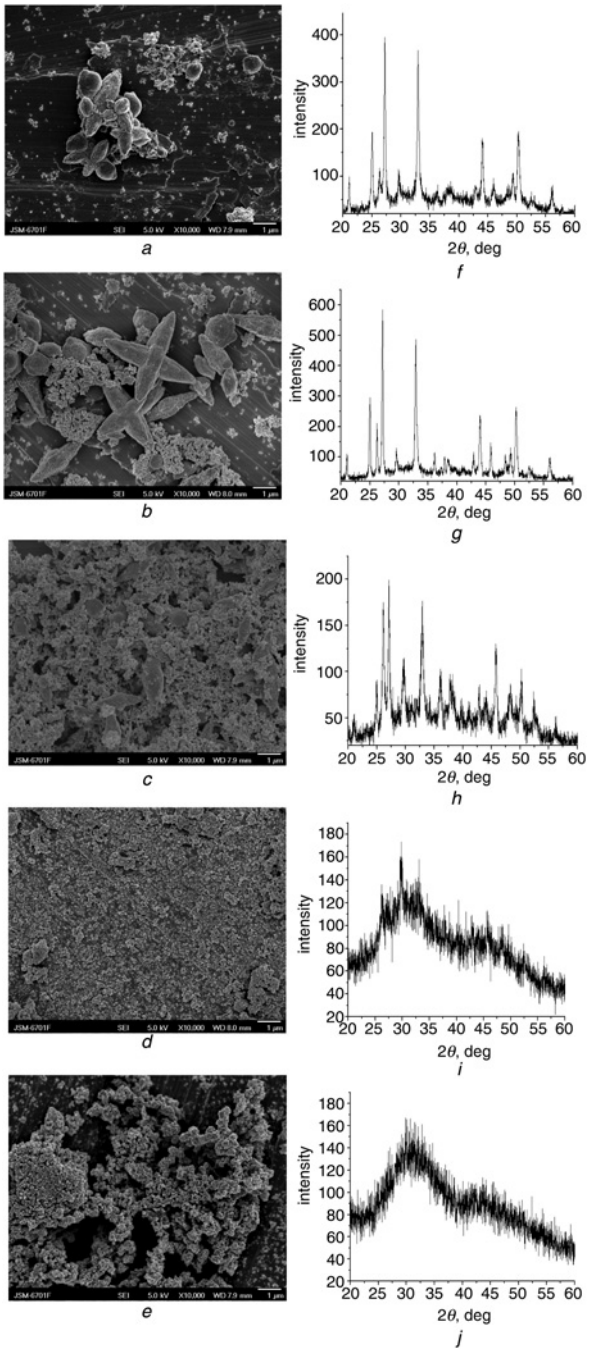

Figure 5 *SEM and XRD images of coprecipitation particles depending on reverse micelle systems with different Mg^{2+}/Ca^{2+} ratios*
a, *f* 1:3
b, *g* 1:2
c, *h* 1:1
d, *i* 2:1
e, *j* 3:1

of unique spherical nanoparticles, ω_0 is the mole ratio of water-to-surfactant content ([H_2O]/[surfactant]) [27]. All the microemulsions were prepared at a ω_0 value of 9.0–9.2, the theoretical calculated values of R_m (the radius of the droplet) at these ω_0 were calculated according to Kang *et al.* [28] and were about 13 nm. Hence, the experimental results of 10–100 nm are also basically consistent with the calculation results of 13 nm.

What causes the formed spherical aggregates to gradually increase when the Ca^{2+}/Mg^{2+} ratio increased? The authors think it could be because of the influence of $MgCO_3$ in $CaCO_3$, and also

Table 3 Molar ratio of Mg^{2+} and Ca^{2+} in the microemulsion and the product

	Mg^{2+}: Ca^{2+}				
microemulsion	1:3	1:2	1:1	2:1	3:1
product	1:4.295	1:2.432	1:1.541	1.988:1	2.545:1

can be explained by the $MgCO_3$ lattice energy and other relevant physicochemical properties [29, 30]. Although the lattice energy of $MgCO_3$ crystal is larger than calcium carbonate crystal, the hydration of magnesium ions is much larger than calcium ions [31], thus making the bonding force between Ca^{2+} larger than the bonding force between Mg^{2+} in an aqueous solution (under the condition of surfactant existing). Therefore, when the content of Ca^{2+} is higher, because of the larger interactions between the calcium ions in the lattice, it is easier to form some fusiform macroaggregate in the solution, but with the content of Ca^{2+} gradually decreased, the Mg^{2+} content increased, and because of the weak interactions between the magnesium ions, it is easier to form uniform dispersed spherical particles.

In addition, we measured the relative content of Mg^{2+} and Ca^{2+} in the product by EDS experiment, and the results are shown in Table 3. We found that the molar proportion of magnesium ions to calcium ions in the product is lower than in the microemulsion. This may be because the solubility of Mg^{2+} is larger than that of Ca^{2+} in an aqueous solution.

The physical and chemical structures of the coprecipitation particles were further analysed by XRD. XRD patterns of calcium carbonate in different concentrations of the Mg^{2+} systems are also displayed in Figs. 5*f*–*j*. The presence of three crystalline polymorphs are indicated, which are aragonite, vaterite and calcite. The diffraction peaks found at 2θ of 26.21°, 33.13°, 36.17°, 37.89°, 42.85°, 45.85° and 52.45°, and are distributed to the (111), (012), (206), (112), (221) and (113) plane diffractions of aragonite crystals, respectively; the peaks found at 2θ of 20.99°, 24.90°, 27.06°, 32.78°, 43.84° and 50.08° are distributed to the (004), (110), (112), (114), (300) and (118) plane diffractions of vaterite crystals, respectively; whereas, the peaks located at 2θ of 29.4°, 35.8°, 42.1° and 48.6° are assigned to the (104), (110), (202) and (116) plane diffractions of calcite crystals, respectively. They are in good agreement with the reported values {JCPDF Cards 47-1743 (calcite) and 33-0268 (vaterite)}.

In Fig. 5*f*, the (110) and (112) diffraction peaks of vaterite are the strongest ones, demonstrating the vaterite is the main crystalline form when Mg^{2+} to Ca^{2+} have a ratio of 1:3, when Mg^{2+} to Ca^{2+} have a ratio of 1:2 and 1:1, the (111) and (012) diffraction peaks of aragonite are the strongest ones, indicating the aragonite is the main crystalline form but with a small amount of vaterite and magnesium calcite, which are shown in Figs. 5*g* and *h*. When the molar proportion of magnesium ions to calcium ions changes to 2:1 and 3:1, the coprecipitation particles are mainly amorphous, which are shown in Figs. 5*i* and *j*. They coincide well with the FTIR experimental results.

Hence, we found that when the proportion of magnesium ions to calcium ions decreases, the relative diffraction peaks intensity analysis shows vaterite is less and less, and aragonite is more and more. However, when the proportion of magnesium ions to calcium ions increased to 2:1, the precipitation form becomes amorphous; after comparing with JCPDF Card 47-1743 we also found there is little calcite and magnesian calcite, which is probably because the magnesian calcite is more soluble than pure calcite and has an inhibitory effect on the formation of calcium carbonate calcite.

4. Conclusions: In this study, we systematically drew a series of inverse-microemulsion quasi-ternary system phase diagrams of CTAB + *n*-butanol + *n*-hexane + brine ($MgCl_2$/$CaCl_2$) by adjusting the ratio of $MgCl_2$ and $CaCl_2$, and calculated the microemulsion region area of the $MgCl_2$/$CaCl_2$ mixed aqueous solution at different mass ratios by using Image-Pro Plus software. We found that they have similar graphical shapes and the areas fluctuated within a range of 14 000–17 000. The coprecipitations were prepared depending on reverse microemulsion; from the SEM graph we found that as the Ca^{2+}/Mg^{2+} ratio increased, the formation of spherical aggregates gradually increased. When the content of Ca^{2+} is higher, it is easier to form some fusiform macroaggregate the solution because of the larger interactions between the calcium ions in the lattice, but with the content of Ca^{2+} gradually decreasing and Mg^{2+} increasing, it is easier to form uniform dispersed spherical granules.

The FTIR spectra and XRD demonstrated that the vaterite is the main crystalline form when Mg^{2+} to Ca^{2+} have a ratio of 1:3; when Mg^{2+} to Ca^{2+} have ratios of 1:2 and 1:1, the aragonite is the main crystalline form but there are small amounts of vaterite and magnesium calcite, and as the proportion of magnesium ions to calcium ions change to 2:1 and 3:1, the coprecipitation particles are mainly amorphous.

5. Acknowledgments: This work was supported by the Science and Technology Support Projects of Gansu Province (grant no. 1204NKCA107), the Engineering and Technology Center Projects of Gansu (grant no. 1106NTGA013), the Major Science and Technology Projects of Gansu (grant no. 1002NKDA025), the Pre-Research Funds of Jinchuan Company-Lanzhou Jiaotong University (grant no. JCYY2013008) and the 'Qing Lan' Talent Engineering Funds of Lanzhou Jiaotong University.

6 References

[1] Lowenstam H.A.: 'Spicular morphology and mineralogy in some Pyuridae (Ascidiacea)', *Bull. Mar. Sci.*, 1989, **45**, pp. 243–252
[2] Zenger D.H.: 'Sedimentary carbonate minerals' (Springer, Berlin, Germany, 1973)
[3] Addadi L., Raz S., Weiner S.: 'Taking advantage of disorder: amorphous calcium carbonate and its role in biomineralization', *Adv. Mater.*, 2003, **15**, pp. 959–970
[4] Schulman J.H., Stoekenius W., Prince L.M.: 'Mechanism of formation and structure of microemulsions by electron microscopy', *J. Phys. Chem.*, 1959, **63**, pp. 1677–1680
[5] Wang C.C., Dong H.C., Huang T.C.: 'Synthesis of palladium nanoparticies in water-in-oil microemulsion', *Colloids Surf. A.*, 2001, **189**, pp. 145–154
[6] Curri M.L., Gostiano A., Mavelli F.: 'Reverse micellar systems: self organized assembly as effective route for the synthesis of colloidal semiconductor nanocrystals', *Mater. Sci. Eng. C.*, 2002, **22**, pp. 423–426
[7] Lu C.H., Saha S.K.: 'Synthesis of ultrafine strontium bismuth tantalate powder by colloid-emulsion technique', *Mater. Lett.*, 2000, **42**, pp. 150–154
[8] Chen D.H., Chen Y.Y.: 'Synthesis of strontium ferrite ultrafine particles using microemulsion processing', *J. Colloid. Interface. Sci.*, 2001, **23**, pp. 41–46
[9] Pillai V., Kumar P.: 'Structure and magnetic properties of nanoparticles of barium ferrite synthesized using microemulsion processing', *Colloids Surf. A*, 1993, **80**, pp. 69–75
[10] Chave K.E.: 'Aspects of the biogeochemistry of magnesium 2. Calcareous marine organisms', *J. Geol.*, 1954, **62**, pp. 587–599
[11] Bischoff W.D., Mackenzie F.T., Bishop F.C.: 'Stabilities of synthetic magnesian calcites in aqueous solution: comparison with biogenic materials', *Geochim. Cosmochim. Acta*, 1987, **51**, pp. 1413–1423
[12] Chave K.E.: 'Aspects of the biogeochemistry of magnesium 1. Calcareous marine organisms', *J. Geol.*, 1954, **62**, pp. 266–283
[13] Yong J.H., Aizenberg J.: 'Effect of magnesium ions on oriented growth of calcite on carboxylic acid functionalized self-assembled monolayer', *J. Am. Chem. Soc.*, 2003, **125**, pp. 4032–4033
[14] Loste E., Wilson R.M., Seshadri R., Meldrum F.C.: 'The role of magnesium in stabilising amorphous calcium carbonate and controlling calcite morphologies', *J. Cryst. Growth*, 2003, **254**, pp. 206–218
[15] Shen F.H., Feng Q.L., Wang C.M.: 'The modulation of collagen on crystal morphology of calcium carbonate', *J. Cryst. Growth*, 2002, **242**, pp. 239–244

doi: 10.1049/mnl.2013.0656

[16] Xu A.W., Yu Q., Dong W.F., Antonietti M., Colfen H.: 'Stable amorphous microparticles with hollow spherical superstructures stabilized by phytic acid', *Adv. Mater.*, 2005, **17**, pp. 2217–2221
[17] Naka K.: 'Effect of dendrimers on the crystallization of calcium carbonate in aqueous solution', *Top. Curr. Chem.*, 2003, **228**, pp. 141–158
[18] Zhao M.Q., Sun L., Crooks R.M.: 'Preparation of Cu nanoclusters within dendrimer templates', *J. Am. Chem. Soc.*, 1998, **120**, pp. 4877–4878
[19] Balogh L., Tomalia D.A.: 'Poly(amidoamine) dendrimer-templated nanocomposites. 1. Synthesis of zerovalent copper nanoclusters', *J. Am. Chem. Soc.*, 1998, **120**, pp. 7355–7356
[20] Groot K.D., Duyvis E.M.: 'Crystal form of precipitated calcium carbonate as influenced by adsorbed magnesium ions', *Nature*, 1966, **212**, pp. 183–184
[21] Folk R.L.: 'The natural of history of crystalline calcium carbonate; effect of magnesium content and salinity', *J. Sedimentol. Pet.*, 1974, **44**, pp. 40–53
[22] Lahann R.W.: 'A chemical model for calcite crystal growth and morphology control', *J. Sedimentol. Pet.*, 1978, **48**, pp. 337–347
[23] Xu X.R., Han J.T., Cho K.: 'Formation of amorphous calcium carbonate thin films and their role in biomineralization', *Chem. Mater.*, 2004, **16**, pp. 1740–1746
[24] Zhang Z.N., Xie Y.D., Xun X.R., Pan H.H., Tang R.K.: 'Transformation of amorphous calcium carbonate into aragonite', *J. Cryst. Growth*, 2012, **343**, pp. 62–67
[25] Tlili M.M., Amor M.B., Gabrielli C., Joiret S., Maurin G., Rousseau P.: 'Characterization of $CaCO_3$ hydrates by micro-Raman spectroscopy', *J. Raman Spectrosc.*, 2002, **33**, pp. 10–16
[26] Neumann M., Epple M.: 'Monohydrocalcite and its relationship to hydrated amorphous calcium carbonate in biominerals', *J. Inorg. Chem.*, 2007, **14**, pp. 1953–1957
[27] Wang N., Wang X.Q., Yang L.J., Chen H.S.: 'The morphology and size control of nano calcium carbonate crystallised in reverse micelle system with cationic surfactant CTAB', *Micro Nano Lett.*, 2013, **8**, pp. 94–98
[28] Kang S.H., Hirasawa I., Kim W.S., Choi C.K.: 'Morphological control of calcium carbonate crystallized in reverse micelle system with anionic surfactants SDS and AOT', *J. Colloid Interface Sci.*, 2005, **288**, pp. 496–502
[29] Glasser L., Jenkins H.D.B.: 'Lattice energies and unit cell volumes of complex ionic solids', *J. Am. Chem. Soc.*, 2000, **122**, pp. 632–638
[30] Mandell G.K., Rock P.A.: 'Lattice energies of calcite structure metal carbonates II. Results for $CaCO_3$, $CdCO_3$, $FeCO_3$, $MgCO_3$ and $MnCO_3$', *J. Phys. Chem. Solid*, 1998, **59**, pp. 703–712
[31] Yang S.H., Wu G.H.: 'Model of ionic hydrate and calculation of hydration energy', *J. Inorg. Chem.*, 1988, **4**, pp. 124–129